J Biomol NMR (2010) 48:59–64
DOI 10.1007/s10858-010-9434-8

NMR STRUCTURE NOTE

NMR structure of the calponin homology domain of human IQGAP1 and its implications for the actin recognition mode

Ryo Umemoto · Noritaka Nishida · Shinji Ogino · Ichio Shimada

Received: 12 June 2010 / Accepted: 1 July 2010 / Published online: 20 July 2010

Biological context

IQ-domain GTPase-activating protein 1 (IQGAP1), a multi-domain protein with a molecular mass of 189 KDa, promotes actin crosslinking at the leading edge of cells, under the control of the small GTPases; Rac1 and Cdc42 (Bashour et al. 1997; Fukata et al. 1997). Previous studies demonstrated that the direct interaction between actin filaments (F-actin) and IQGAP1 is essential for the promotion of cell migration (Mataraza et al. 2007). This interaction is mediated through an N-terminal actin-binding domain (ABD) (residues 1–210), which contains a calponin homology (CH) domain (Mateer et al. 2004). CH domains are commonly found in many other actin-binding proteins (Gimona et al. 2002; Sjoblom et al. 2008). Most of the actin-binding proteins, such as filamin and dystrophin, contain tandem CH domains, referred to as CH1 and CH2 domains, which work together to recognize F-actin. On the other hand, IQGAP1 is classified in the type 3 CH family, which contains a single CH domain. The actin-recognition mechanism of the type 3 CH domain family has been poorly characterized thus far (Bramham et al. 2002). In addition, IQGAP1 requires the flanking N and C-terminal segments of the CH domain to form a functional F-actin binding domain. As a first step toward understanding the mechanism of the actin-recognition by the single CH domain family, we solved the NMR structure of the actin binding domain of IQGAP1.

R. Umemoto · N. Nishida · S. Ogino · I. Shimada (✉)
Graduate School of Pharmaceutical Sciences, The University of Tokyo, Hongo, Bunkyo-ku, Tokyo 113-0033, Japan
e-mail: shimada@iw-nmr.f.u-tokyo.ac.jp

R. Umemoto · S. Ogino
Japan Biological Informatics Consortium, Aomo, Koto-ku, Tokyo 135-8073, Japan

I. Shimada
Biomedicinal Information Research Center, National Institute of Advanced Industrial Science and Technology, AIST, Aomi, Koto-ku, Tokyo 135-0064, Japan

Methods and results

Protein expression and purification

The cDNA fragments corresponding to human IQGAP1 ABD (1–210) and ABD (26–210) were separately cloned into the pGEX-6p vector (GE Healthcare). The ^{13}C- and ^{15}N-labeled proteins were expressed by the *E. coli* strain BL21 (DE3), grown in M9 minimal medium containing $^{15}NH_4Cl$ (1 g/l) and ^{13}C-glucose (2 g/l) as the sole nitrogen and carbon sources. The cells were cultured to an OD_{600} of 0.8 at 37°C, and the protein expression was induced with isopropyl-D-1-thiogalactopyranoside (final concentration of 0.4 mM) for 4 h at 25°C. The ABDs were purified on a glutathione-Sepharose 4B column (GE Healthcare), and the GST tag was excised from the ABDs with PreScission protease (GE Healthcare). The ABDs were further purified on a Superdex 75 gel filtration column (GE Healthcare).

Construct design of the ABDs

According to the previous report, we first prepared the ABD containing residues 1–210. The ^{1}H-^{15}N HSQC spectrum of ABD (1–210) exhibited a cluster of strong resonances in the center, indicating that the protein contains unstructured segments (black, Fig. 1a). Therefore, we prepared the truncated version of the ABD (26–210)

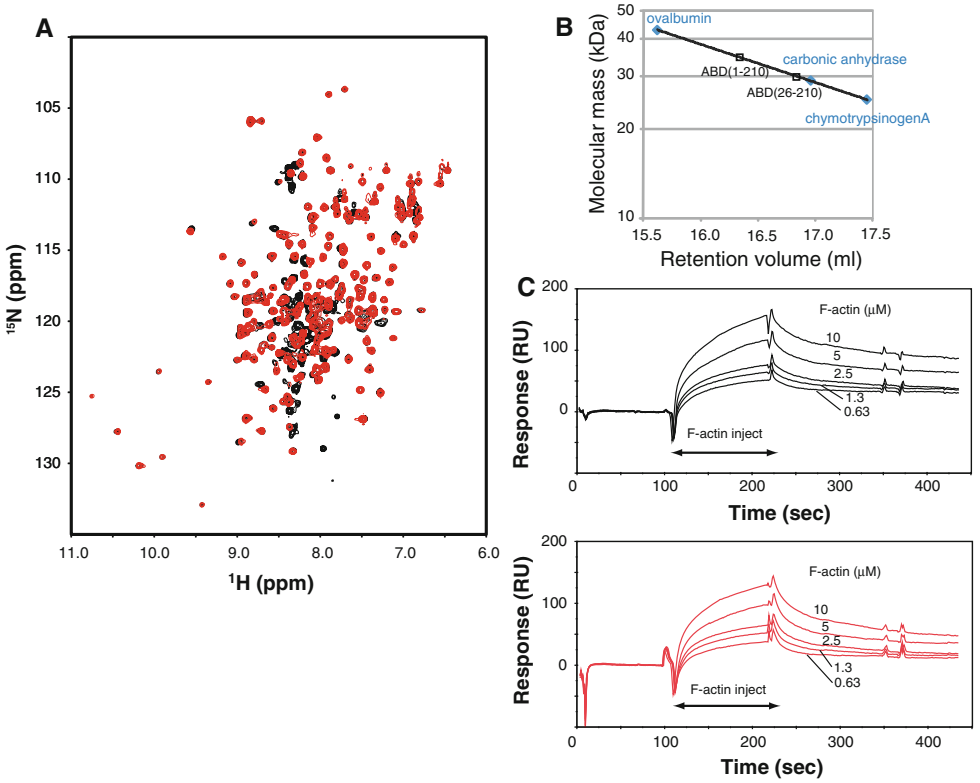

Fig. 1 Structural and functional characterization of ABDs. **a** Overlaid ^{1}H-^{15}N HSQC spectra of ABD (1–210) (*black*) and ABD (26–210) (*red*). **b** Analytical size exclusion chromatography of the ABDs. The elution volumes of the ABD constructs are plotted with squares. The standard curve was drawn from the elution volumes of ovalbumin (43 kDa), carbonic anhydrase (29 kDa), and chymotrypsinogen A (25 kDa). **c** SPR sensorgrams of F-actin binding to ABD (1–210) (*black*) and ABD (26–210) (*red*) immobilized on a CM5 sensor chip. The concentrations of F-actin are indicated in each sensorgram

construct, based on the limited trypsin proteolysis. The peak appearing in the center of the spectrum was significantly reduced with ABD (26–210) (red, Fig. 1a).

Size exclusion chromatography

The purified ABDs were examined by the size exclusion chromatography, using a Superdex200 10/300 GL gel filtration column (GE Healthcare) preequibrated with the buffer containing 20 mM sodium phosphate, pH 7.4, 150 mM NaCl, and 1 mM DTT. The molecular mass was estimated by comparison with the elution volumes of the following standard proteins: ovalbumin (43 kDa), carbonic anhydrase (29 kDa), and chymotrypsinogen A (25 kDa) (Fig. 1b).

The elution volumes of ABD (1–210) and ABD (26–210) were 16.38 and 16.88 ml, respectively. Assuming a globular shape, the molecular masses of ABD (1–210) and ABD (26–210) were estimated to be 34 and 30 kDa, respectively. The estimated molecular masses are larger than the theoretical molecular masses [24.6 kDa for ABD (1–210) and 22.0 kDa for ABD (26–210)], but smaller than those of the dimers. As described below, ABD (1–210) and ABD (26–210) each contain a flexible N-terminal segment, which may account for the increased the hydrodynamic radius. Therefore, we concluded that the ABDs exist as monomeric proteins in solution (Fig. 1b).

Surface plasmon resonance (SPR)

The actin binding activities of the ABDs were analyzed by SPR measurements, using a BIAcore 2000 instrument (GE Healthcare). The ABDs were immobilized on the sensor chip CM5 using standard amine-coupling chemistry, resulting in a signal of 3,000–3,500 resonance units. On the control flow cell, the same amount of BSA was immobilized using the same method. The binding assay was performed in running buffer (5 mM Tris, pH 7.4, 50 mM KCl, 2 mM $MgCl_2$ 0.2 mM $CaCl_2$, 1 mM DTT, 1 mM ATP, 0.05% Tween 20) at a flow rate of 20 μl/min, using serial dilutions of F-actin in the 0.63–10 μM range. The sensorgrams of the BSA immobilized chip were subtracted from those of the ABD immobilized chip to remove non-specific interactions of F-actin to the sensor chip. The bound F-actin was removed from the chip surface by microinjections of regeneration buffer (5 mM NaOH, 1 mM DTT).

The subtracted response curves of the F-actin injections were similar between ABD (1–210) and ABD (26–210) (Fig. 1c). Therefore, we used the ABD (26–210) construct for further structural analysis. It should be noted that the interaction observed here reflects the multivalent interaction between the immobilized ABD and the F-actin in flow, precluding further quantitative analysis.

Table 1 Structural statistics of IQGAP1 ABD (26–210)

NOE distance constraints	
Short-range ($\|i - j\| \leq 1$)	1,215
Medium-range ($2 \leq \|i - j\| \leq 4$)	415
Long-range ($\|i - j\| \geq 5$)	504
Total	2,134
Hydrogen bonds	48
Dihedral angle restraints	
HNHA (Φ)	43
TALOS (Φ and Ψ)	134
Ramachandran statistics (%)	
Residues in most favored regions	80.5
Residues in additionally allowed regions	19.0
Residues in generously allowed regions	0.5
Residues in disallowed regions	0.0
Root mean square deviations from the average structure[a] (Å)	
Backbone atoms	0.62 ± 0.13
Heavy atoms	1.09 ± 0.10

[a] Calculated using residues 39–58, 65–71, 75–84, 114–126, 136–140, 146–160, 178–189

NMR spectroscopy

All NMR spectra (0.90 mM protein in 20 mM sodium phosphate, pH 7.4, 150 mM NaCl, 1 mM DTT, 1 mM NaN_3, 90% H_2O, 10% D_2O) were recorded at 37°C with a Bruker Avance 800 spectrometer equipped with a cryogenic probe. The solvent was replaced with 100% D_2O for recording the ^{13}C-NOESY-HSQC, HC(C)H-TOCSY, (H)CCH-TOCSY and HC(C)H-COSY spectra, and for the ^{1}H-^{15}N HSQC spectrum for hydrogen–deuterium exchange. Sequential assignments of the backbone resonances of the ABD were achieved using the following triple resonance experiments recorded on a uniformly ^{13}C, ^{15}N-labeled sample in H_2O buffer: HNCA, HNCACB, CBCA(CO)NH, HNCO, and HN(CA)CO. Side-chain resonances were assigned on the basis of triple resonance experiments, HBHA(CO)NH, H(CCO)NH, (H)C(CO)NH, HC(C)H-TOCSY, (H)CCH-TOCSY and HC(C)H-COSY (Clore and Gronenborn 1994). Aromatic side-chain resonances were assigned on the basis of HbCbCgCdHd, and HbCbCgCdCeHe (Yamazaki et al.

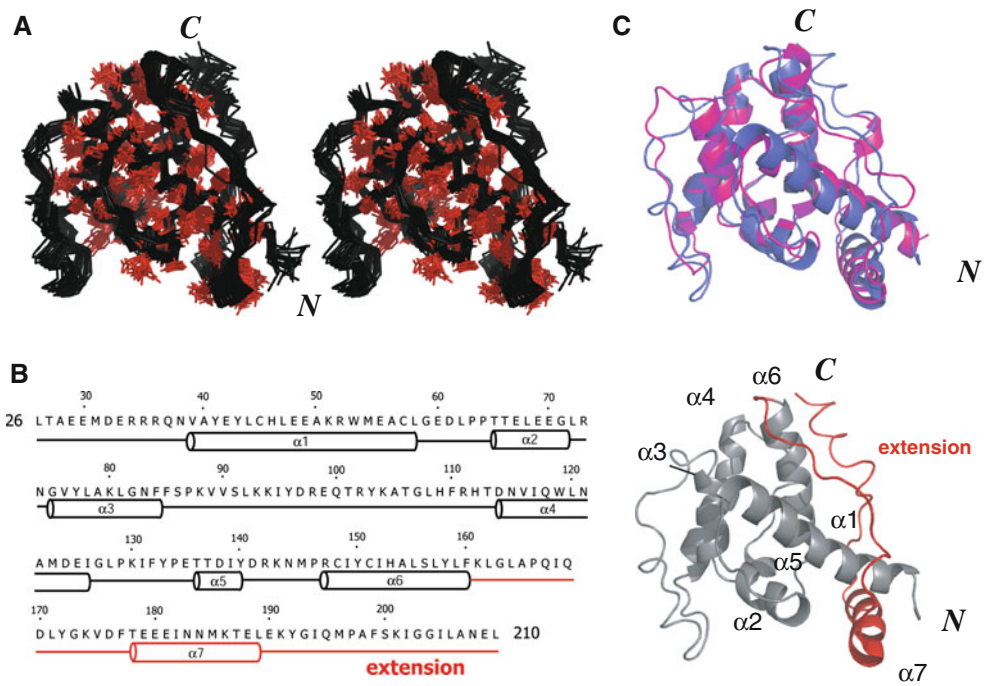

Fig. 2 Solution structure of ABD. **a** Stereoviews of the overlaid ensemble of the 20 final structures. The side chains in the structured region (39–58, 65–71, 75–84, 114–126, 136–140, 146–160, and 178–189) are colored *red*. The N-terminal disordered region (residues 26–34) is not shown. **b** The primary sequence and a ribbon diagram of the ABD (26–210). The α-helices are depicted as *cylinders* in the sequence. In the ribbon diagram, the CH domain is colored *black*, and the following additional segment (161–210), which we refer to as the "extension", is colored *red*. **c** Overlay of the structures of the IQGAP1 ABD (*blue*) and Rng2, a yeast homologue of IQGAP1 (*purple*, PDB code 1P2X). The structures were drawn using the PyMOL software (DeLano 2008)

1993). All spectra were processed by XWIN-NMR or Topspin (Bruker Biospin) and were analyzed by Sparky (Kneller and Goddard 1997).

Structure calculation

Approximate interproton distances were obtained from the ^{13}C-NOESY-HSQC, ^{15}N-NOESY-HSQC, ^{13}C-HSQC-NOESY-^{13}C-HSQC and ^{13}C-HSQC-NOESY-^{15}N-HSQC spectra. The mixing time was 100 ms for all NOESY experiments. A series of ^{1}H-^{15}N HSQC spectra was acquired on a sample freshly dissolved in D_2O, to identify the slowly exchanging amides. Amides that had not exchanged after 3 h and that were located in regions of defined secondary structure, based on the NOE data, were restrained to form HN–CO hydrogen bonds, using the distance restraints of 2.4–3.3 Å for O–N and 1.5–2.3 Å for O–HN, respectively. For structure calculations, 96 restraints were used for 48 backbone hydrogen bonds. In addition, dihedral angle constraints based on the HNHA (Vuister and Bax 1993) and TALOS (Cornilescu et al. 1999, Shen et al. 2009) were used. CYANA v. 2.1 was used to compute seven cycles, each with 100 conformers (Herrmann et al. 2002). Input data and structure calculation statistics are summarized in Table 1. The final ensemble of 20 structures was selected based on the CYANA target function values. A Ramachandran plot of the final 20 structures, calculated using PROCHECK v. 3.4.4, showed 80.5, 19.0, 0.5, and 0.0% of the residues in the most favored, additionally allowed, generously allowed, and disallowed regions, respectively (Laskowski et al. 1993). The structure coordinates and the chemical shift data have been deposited in the Protein Data Bank (PDB code: 2RR8) and the BMRB (BMRB code: 11175), respectively.

Discussion and conclusions

Structure of IQGAP1 ABD

The three-dimensional structure of the ABD (26–210) was determined, using standard heteronuclear multidimensional

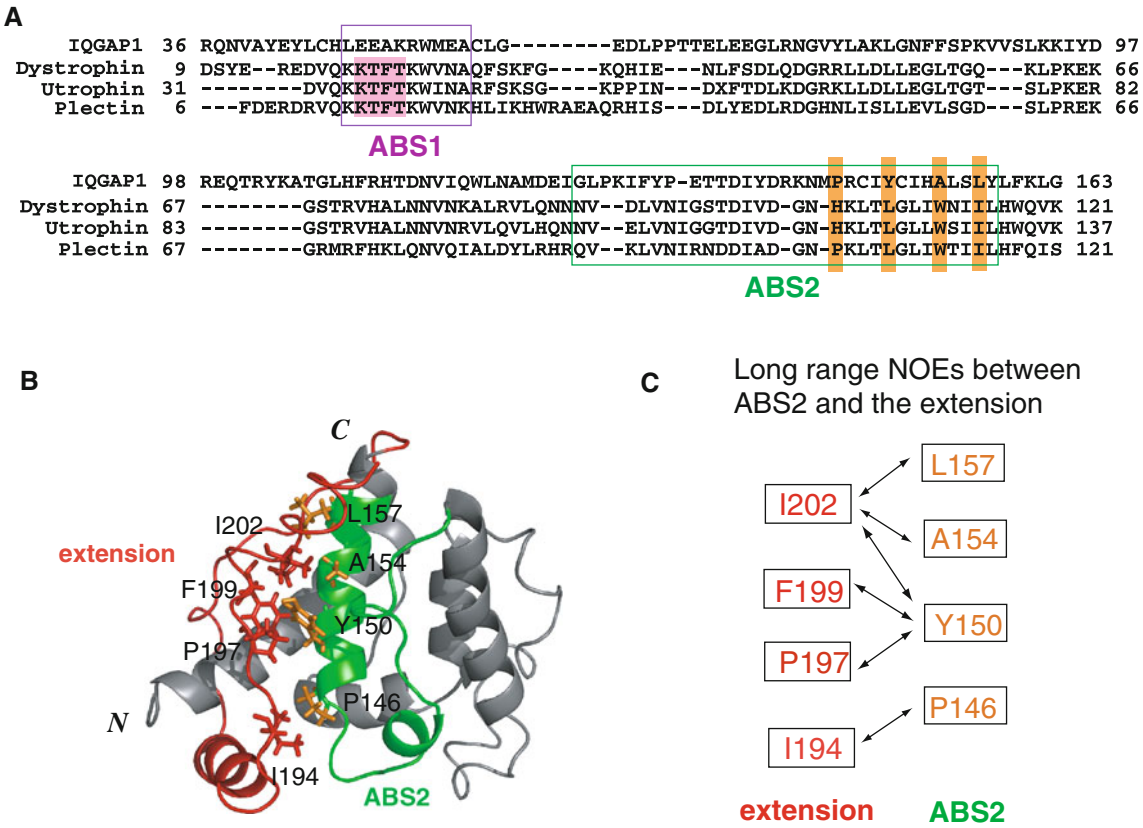

Fig. 3 Potential actin binding sites of IQGAP1 ABD. **a** A structure-based sequence alignment of IQGAP1 ABD with other actin-binding CH domains. The regions corresponding to ABS1 and ABS2 are indicated by the *purple* and *green boxes*, respectively. The KTFT sequence is highlighted in pink, and the hydrophobic residues in the α6 helix of ABS2 are highlighted in *orange*. **b** Ribbon diagram of ABD of IQGAP, in which ABS2 and the extension are colored *green* and *red*, respectively. Long-range NOEs are observed between the residues in ABS2 (shown as *red sticks*) and the residues in the extension (shown as *orange sticks*). **c** Schematic drawing of the interacting residues of ABS2 and the extension. The residues from ABS2 and the extension are colored *orange* and *red*, respectively

NMR (see "Methods and results"). The final 20 structures of the IQGAP1 ABD were superimposed with respect to each other in Fig. 2a. The poorly converged N-terminal segment up to residue 34 seems to be an unstructured region. The overall fold of ABD (26-210) consists of seven α-helices, α1–α7 (α1, 39–58; α2, 65–71; α3, 75–84; α4, 114–126; α5, 137–140; α6, 146–160; α7, 178–189). The first 6 helices comprise the CH domain, which is conserved among other actin-binding proteins. The following segment (residues 161–210), termed the "extension" region, is composed of long loops that contain a short α-helix in the middle, and makes intimate contacts with the CH domain moiety (Fig. 2b). A comparison with the crystal structure of Rng2 (Wang et al. 2004), a yeast homologue of IQGAP1, revealed that the overall fold of the IQGAP1 ABD is mostly similar (Fig. 2c).

Potential actin-binding site

Previous studies identified the two potential actin binding sites (termed ABS1 and ABS2) in the CH1 domain (Kuhlman et al. 1992; Levine et al. 1990, 1992). In ABS1, the KTFT sequence is reportedly important for actin binding (Levine et al. 1990). However, this sequence is not conserved in the IQGAP1 CH domain (Fig. 3a). On the other hand, the hydrophobic residues in the α6 helix known as ABS2 (highlighted in orange), are conserved in the IQGAP1 sequence (Fig. 3a). Therefore, we hypothesized that these conserved residues (P146, Y150, A154, and L157) form an actin-interacting surface. However, ABS2 of the IQGAP1 ABD is not exposed to the solvent (Fig. 3b). The extensive NOE connectivity between ABS2 and the extension segment supports the proposal that the potential actin-binding residues of IQGAP1 ABD are masked by the extension (Fig. 3c). Based upon this evidence, we developed two hypotheses for the recognition mode of F-actin. First, the actin binding site of the IQGAP1 CH domain is not in ABS2, and the other region is responsible for the actin-binding. Second, the actin-recognition is accompanied by some conformational changes that unmask the extension and expose ABS2 to the solvent. It should be noted that such an "opening" mechanism is proposed in the case of the tandem CH domains of α-actinin (Galkin et al. 2010). However, in either case, further studies are necessary to clarify the recognition mode of F-actin by the IQGAP1 ABD.

Conclusions

Although a number of tandem actin binding CH domains have been reported, the IQGAP1 ABD is the first example of the type 3 single CH domain, which shows actin binding activity. Our NMR structure of the ABD of IQGAP1 revealed that the putative actin binding site, termed ABS2, is masked by the extension. Therefore, the actin binding mechanism may differ from those other tandem CH domains, which recognize F-actin directly via ABS2. Although the mechanism by which IQGAP1 ABD binds to F-actin remains to be elucidated, the ABD structure reported here will be useful for structure-based studies of the interaction between F-actin and the IQGAP1 ABD.

Acknowledgments This work was supported by grants from the Japan New Energy and Industrial Technology Development Organization and the Ministry of Economy, Trade, and Industry.

References

Bashour AM, Fullerton AT, Hart MJ, Bloom GS (1997) IQGAP1, a Rac- and Cdc42-binding protein, directly binds and cross-links microfilaments. J Cell Biol 137:1555–1566

Bramham J, Hodgkinson JL, Smith BO, Uhrin D, Barlow PN, Winder SJ (2002) Solution structure of the calponin CH domain and fitting to the 3D-helical reconstruction of F-actin:calponin. Structure 10:249–258

Clore GM, Gronenborn AM (1994) Multidimensional heteronuclear nuclear magnetic resonance of proteins. Methods Enzymol 239:349–363

Cornilescu G, Delaglio F, Bax A (1999) Protein backbone angle restraints from searching a database for chemical shift and sequence homology. J Biomol NMR 13:289–302

DeLano WL (2008) The PyMOL molecular graphics system. DeLano Scientific LLC, Palo Alto, CA, USA. http://www.pymol.org

Fukata M, Kuroda S, Fujii K, Nakamura T, Shoji I, Matsuura Y, Okawa K, Iwamatsu A, Kikuchi A, Kaibuchi K (1997) Regulation of cross-linking of actin filament by IQGAP1, a target for Cdc42. J Biol Chem 272:29579–29583

Galkin VE, Orlova A, Salmazo A, Djinovic-Carugo K, Egelman EH (2010) Opening of tandem calponin homology domains regulates their affinity for F-actin. Nat Struct Mol Biol 17:614–616

Gimona M, Djinovic-Carugo K, Kranewitter WJ, Winder SJ (2002) Functional plasticity of CH domains. FEBS Lett 513:98–106

Herrmann T, Guntert P, Wuthrich K (2002) Protein NMR structure determination with automated NOE assignment using the new software CANDID and the torsion angle dynamics algorithm DYANA. J Mol Biol 319:209–227

Kneller DG, Goddard TD (1997) SPARKY 3.105 edit. University of California, San Francisco

Kuhlman PA, Hemmings L, Critchley DR (1992) The identification and characterisation of an actin-binding site in alpha-actinin by mutagenesis. FEBS Lett 304:201–206

Laskowski RA, MacArthur MW, Moss DS, Thornton JM (1993) PROCHECK: a program to check the stereochemical quality of protein structures. J Appl Crystallogr 26:283–291

Levine BA, Moir AJ, Patchell VB, Perry SV (1990) The interaction of actin with dystrophin. FEBS Lett 263:159–162

Levine BA, Moir AJ, Patchell VB, Perry SV (1992) Binding sites involved in the interaction of actin with the N-terminal region of dystrophin. FEBS Lett 298:44–48

Mataraza JM, Li Z, Jeong HW, Brown MD, Sacks DB (2007) Multiple proteins mediate IQGAP1-stimulated cell migration. Cell Signal 19:1857–1865

Mateer SC, Morris LE, Cromer DA, Bensenor LB, Bloom GS (2004) Actin filament binding by a monomeric IQGAP1 fragment with a single calponin homology domain. Cell Motil Cytoskeleton 58:231–241

Shen Y, Delaglio F, Cornilescu G, Bax A (2009) TALOS+: a hybrid method for predicting protein backbone torsion angles from NMR chemical shifts. J Biomol NMR 44:213–223

Sjoblom B, Ylanne J, Djinovic-Carugo K (2008) Novel structural insights into F-actin-binding and novel functions of calponin homology domains. Curr Opin Strurct Biol 18:702–708

Vuister GW, Bax A (1993) Quantitative J correlation: a new approach for measuring homonuclear three-bond J(HNH.alpha.) coupling constants in 15N-enriched proteins. J Am Chem Soc 115:7772–7777

Wang CH, Balasubramanian MK, Dokland T (2004) Structure, crystal packing and molecular dynamics of the calponin-homology domain of Schizosaccharomyces pombe Rng2. Acta Crystallogr D Biol Crystallogr 60:1396–1403

Yamazaki T, Forman-Kay JD, Kay LE (1993) Two-dimensional NMR experiments for correlating 13Cβ and 1Hδ/ε chemical shifts of aromatic residues in 13C-labeled proteins via scalar couplings. J Am Chem Soc 115:11054–11055